

Charge-changing-cross-section measurements of $^{12-16}\text{C}$ at around 45A MeV and development of a Glauber model for incident energies 10A – 2100A MeV

D.T. Tran,^{1,2,*} H.J. Ong,^{1,†} T.T. Nguyen,^{3,4} I. Tanihata,^{1,5} N. Aoi,¹ Y. Ayyad,¹ P.Y. Chan,¹ M. Fukuda,⁶ T. Hashimoto,⁷ T.H. Hoang,^{1,2} E. Ideguchi,¹ A. Inoue,¹ T. Kawabata,⁸ L.H. Khieu,² W.P. Lin,⁹ K. Matsuta,⁶ M. Mihara,⁶ S. Momota,¹⁰ D. Nagae,¹¹ N.D. Nguyen,¹² D. Nishimura,¹³ A. Ozawa,¹¹ P.P. Ren,⁹ H. Sakaguchi,¹ J. Tanaka,¹ M. Takechi,¹⁴ S. Terashima,⁵ R. Wada,^{15,9} and T. Yamamoto¹

(RCNP-E372 collaboration)

¹Research Center for Nuclear Physics, Osaka University, Osaka, Japan.

²Institute Of Physics, Vietnam Academy of Science and Technology, Hanoi, Vietnam.

³Pham Ngoc Thach University of Medicine, HCM, Vietnam

⁴Faculty of Physics and Engineering Physics, VNU-HCMUS, HCM, Vietnam.

⁵School of Physics and Nuclear Energy Engineering and IRCNPC, Beihang University, Beijing, China.

⁶Department of Physics, Osaka University, Osaka, Japan.

⁷Institute for Basic Science, Daejeon, Korea.

⁸Department of Physics, Kyoto University, Kyoto, Japan.

⁹Institute of Modern Physics, Lanzhou, China.

¹⁰Kochi University of Technology, Kochi, Japan.

¹¹Institute of Physics, University of Tsukuba, Tsukuba, Japan.

¹²Dong Nai University, Dong Nai, Vietnam.

¹³Tokyo University of Science, Tokyo, Japan.

¹⁴Graduate School of Science and Technology, Niigata University, Niigata, Japan.

¹⁵Cyclotron Institute, Texas A&M University, College Station, Texas, USA.

(Dated: August 31, 2018)

We have measured for the first time the charge-changing cross sections (σ_{CC}) of $^{12-16}\text{C}$ on a ^{12}C target at energies below 100A MeV. To analyze these low-energy data, we have developed a finite-range Glauber model with a global parameter set within the optical-limit approximation which is applicable to reaction cross section (σ_R) and σ_{CC} measurements at incident energies from 10A to 2100A MeV. Adopting the proton-density distribution of ^{12}C known from the electron-scattering data, as well as the bare total nucleon-nucleon cross sections, and the real-to-imaginary-part ratios of the forward proton-proton elastic scattering amplitude available in the literatures, we determine the energy-dependent slope parameter β_{pn} of the proton-neutron elastic differential cross section so as to reproduce the existing σ_R and interaction-cross-section data for $^{12}\text{C}+^{12}\text{C}$ over a wide range of incident energies. The Glauber model thus formulated is applied to calculate the σ_R 's of ^{12}C on a ^9Be and ^{27}Al targets at various incident energies. Our calculations show excellent agreement with the experimental data. Applying our model to the σ_R and σ_{CC} for the “neutron-skin” ^{16}C nucleus, we reconfirm the importance of measurements at incident energies below 100A MeV. The proton root-mean-square radii of $^{12-16}\text{C}$ are extracted using the measured σ_{CC} 's and the existing σ_R data. The results for $^{12-14}\text{C}$ are consistent with the values from the electron scatterings, demonstrating the feasibility, usefulness of the σ_{CC} measurement and the present Glauber model.

PACS numbers: 21.10.Gv, 24.10.-i, 25.60.Dz

INTRODUCTION

The nuclear sizes, usually defined by the root-mean-square (rms) charge or nucleon/matter distribution radii, are important nuclear quantities. The proton and neutron rms radii are not only important to extract information on the nuclear structure, but are also essential for extracting the neutron skin thickness, which offers an important means to constrain theoretical descriptions of the equation of state (EOS) of asymmetric nuclear matter [1]. The nuclear EOS is important to understand the properties of dense nuclear matter such as the neutron stars as well as to predict supernovae and neutron star mergers [2].

Historically, the earliest evidence for a nuclear radius

came not from a direct measurement, but was inferred from the studies of the α decay of radioactive nuclei [3]. It was only after 1950s, with the advent of particle accelerators and the quantum electrodynamic theory, that decisive evidences for finite nuclear sizes and more precise measurements of charge/proton radii became available. Scores of charge radii of mostly stable nuclei have since been precisely determined using electromagnetic probes such as the elastic scattering of fast electrons, X-ray spectroscopy of muonic atom, optical and K_α X-ray isotope-shift (IS) methods [4].

For short-lived unstable nuclei, the IS method had been the only source of information until very recently. The electron scattering which has been the most successful method to determine the nuclear charge radii is not

applicable because the short-lived nuclei are not available as targets. While the effort to perform electron scattering on unstable nuclei is being pursued [5], it may take some time to achieve practical applications. The optical IS method, on the other hand, requires only a small number of atoms of the unstable nuclei. Experimentally, the IS measurements using laser spectroscopy have achieved very high precision (below 100 kHz) and sensitivity [6]. Spurred on by recent advances in computational methods, the IS methods have been successfully applied to determine the charge radii of light unstable nuclei up to ^{12}Be [7–12]. However, it is extremely challenging to apply the IS method to the $10 > Z > 4$ nuclei due mainly to insufficient precision in the atomic physics calculations and difficulty of production of low-energy isotopes.

In terms of other non-electromagnetic probe, an important breakthrough was achieved in 1985 through the measurements of interaction cross sections of light neutron-rich nuclei, which led not only to the discovery of the neutron-halo structure [13] but also to the renaissance in nuclear physics with radioactive beams. Applying the Glauber model [14], the nuclear matter rms radii of neutron-rich He, Li and Be isotopes were extracted for the first time [13]. Since then, interaction (σ_I) as well as reaction cross sections (σ_R) have been extensively measured, providing a wealth of information on the rms radii of the nuclear matter distribution of unstable nuclei up to the proton and neutron driplines [15]. Recently, extending the Glauber-type analysis to the measured charge-changing cross section (σ_{CC}), which is the total cross sections of all processes that change the proton number of a nucleus, I. Tanihata demonstrates [16], through comparisons with the results from the IS method, the feasibility of the σ_{CC} measurements to determine the point-proton distribution rms radii (referred to as “proton rms radii” hereinafter). Combining σ_R and σ_{CC} (or the proton rms radii determined by other electromagnetic probe), it is possible to determine the neutron distribution rms radii. The successful applications of the method to neutron-rich Be [17], B [18] and C [19] isotopes at incident-beam energy higher than 200A MeV mark an important milestone in the studies of nuclear radii.

The Glauber model has been the most widely used and successful method to determine matter rms radii of unstable nuclei. However, the applicability of this method at low-incident energies has been questionable. While the optical-limit approximation (OLA) of the Glauber model under the zero-range approximation (ZR) has proven to be the most economic and convenient model to calculate σ_I or σ_R at high incident energies [15], it failed to reproduce the experimental data at energies below 100A MeV. The discrepancy reaches almost 20% at a few tens of MeV per nucleon for the carbon isotopes [20]. This discrepancies could be due to various possible effects such as the Fermi motion, Pauli correlations [21], and short-range dynamic correlations. Taking into account the higher-order

multiple scattering and Fermi-motion effects, M. Takechi *et al.* [22] modified the bare nucleon-nucleon interaction cross sections and obtained calculations that reproduce the experimental σ_R 's relatively well over a wide range of incident energies. B. Abu-Ibrahim and Y. Suzuki [23], on the other hand, pointed out that the above-mentioned various effects would have been automatically included to some extent in formulating the profile function for the N - N scatterings.

In this paper, we report on the first measurement of the Charge-Changing cross sections (σ_{CC}) of $^{12-16}\text{C}$ on a ^{12}C target at incident energies at around 45A MeV. To analyze the data and extract the proton rms radii, we have developed a Glauber model within the optical-limit approximation (OLA), which is applicable to a wide energy range between 10A and 2100A MeV. Here, we determine the energy-dependent slope parameter β_{pn} of the proton-neutron elastic differential cross section, which is the only missing parameter besides the density distributions required in the Glauber model calculation. The β_{pp} parameter values for proton-proton scattering were adopted from the proton-proton scattering data. The extension of Glauber model to energies below 100A MeV is important because of the sensitivity of the low-energy σ_R (and perhaps σ_{CC}) to the tail-density distributions of halo and skin nuclei. Such sensitivity has been demonstrated by the σ_R 's of ^{11}Be on a ^{12}C and a ^{27}Al [24], as well as of ^{16}C on a ^{12}C target [25]. Applying the present Glauber model to calculate the reaction cross sections of the ^{12}C on a ^9Be and ^{27}Al targets, we demonstrate the reliability of our model. We also show that the extracted proton rms radii for $^{12-14}\text{C}$ are consistent with the results from the electron scatterings.

EXPERIMENT

The experiment was performed at the EN course [26], Research Center for Nuclear Physics (RCNP), Osaka University. Secondary $^{12-16}\text{C}$ beams were produced in separate runs by fragmentation of a ^{22}Ne primary beam at 80A MeV incident on a ^9Be target with thickness ranging from 1.0 - 5.0 mm. The carbon isotope of interest was selected in flight by setting the appropriate magnetic rigidities of two dipole magnets of the EN fragment separator. A flat aluminum degrader, with thickness ranging from 0.3 - 5.0 mm, was placed at the first momentum-dispersive focal plane (F1) to improve the isotope separation of the secondary beams. The momentum acceptances of the secondary beams were typically set to $\pm 0.2\%$ using a set of collimators at F1. The secondary beams were angular focused at the second focal plane (F2), which is a momentum-achromatic and a charge-mass dispersive focal plane. The selected carbon-isotope beam was further purified using a set of collimators at F2 before being transported to and directed onto

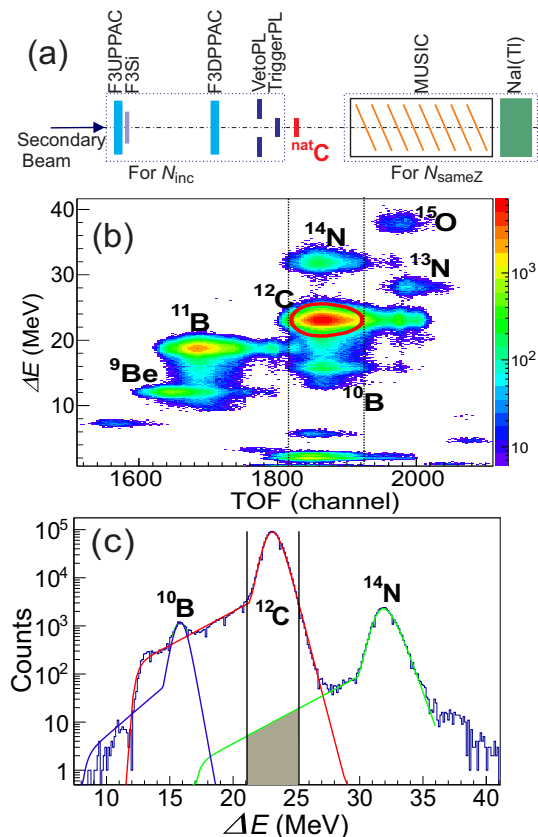


FIG. 1. (Color online). (a) Schematic view of the experiment setup, (b) in-coming ^{12}C beam identification, and (c) contaminant estimation.

a 450-mg/cm²-thick natural carbon target (reaction target) placed at the newly-constructed third focal plane (F3) [27].

In the present work, we measured the σ_{CC} 's of carbon isotopes employing the transmission method. Figure 1(a) shows the experimental setup at F3. The incoming carbon-isotope beam was identified on an event-by-event basis using the energy-loss (ΔE) and time-of-flight (TOF) method. ΔE was measured using a 320- μm -thick silicon detector, while the TOF between the ^9Be production target and the reaction target was determined using the timing information from a 100- μm -thick plastic scintillator placed right before the reaction target and the RF signal from the cyclotron. The timing signal from the plastic scintillator was also used as the trigger for the data-acquisition system. Incident particles were tracked using the position information obtained with four Parallel Plate Avalanche Counters (PPACs) [28] located before F2 and F3. To select and define “good” incident carbon-isotope, we rejected the particles that scattered at large angles after the last PPAC using a 3-mm-thick “veto” plastic scintillator, which has a square hole of a size smaller than the reaction target at its center, placed before the trigger scintillator. The number of “good” in-

cident particles thus counted is denoted by N_{inc} .

The outgoing particles went through a MUlti Sampling Ionization Chamber (MUSIC) [29], which consists of eight anodes and nine cathodes, before being stopped in a 7-cm-thick NaI(Tl) scintillator. The $\Delta E - E$ method was employed to identify and count the scattered particles. The Z -unchanged particles are counted and denoted by $N_{\text{same}Z}$.

DATA ANALYSIS AND RESULTS

In the transmission method, the σ_{CC} is calculated as follows: $\sigma_{\text{CC}} = \ln[\gamma_0/\gamma]/t$, where, t is the number of target nuclei per cm² of beam area, and γ and γ_0 are the ratios of the number of the Z -unchanged particles and the number of incident particles, $\gamma = N_{\text{same}Z}/N_{\text{inc}}$, of measurements with and without the reaction target respectively.

We determined the N_{inc} and $N_{\text{same}Z}$ using the information from the detectors before and after the reaction target respectively. Figure 1(b) shows a typical ΔE -TOF scatter plot for the secondary beams; the red ellipse shows the Particle-IDentification (PID) gate for ^{12}C . The contaminant in the PID gate was mainly the heavier isotopes with reduced energy losses due to the channelling effect in the silicon crystal. To estimate the amount of contaminant, we selected the TOF region as shown by the dotted lines in Fig. 1(b) and projected onto the ΔE axis. Fig. 1(c) shows the projected ΔE distribution for the three nuclides with long tails due to the channeling effect. By scaling the distribution in Fig. 1(c) to N_{inc} , the contaminant was estimated to be less than 0.6% of N_{inc} . The admixtures were further identified and confirmed using the detectors after the reaction target. Depending on the statistics of the carbon isotopes, the contaminants contribute to systematic uncertainties of only about 0.1 – 3.5 mb in the final cross sections, and are much smaller than the errors of the cross sections.

The detection and particles identification of the Z -unchanged particles in the present reaction energies are more complicated than in the high energy due to energy loss straggling and multiple scatterings of the outgoing charged particles in the target and detector materials. The former results in broadening of the measured energy losses while the latter in reduced geometrical acceptance for the scattered-particle detectors. Figure 2(a) shows a typical $\Delta E - E$ plot for scattered particles obtained with the MUSIC (ΔE) and NaI(Tl) scintillator (E). The particles are classified by 7 regions as shown in the figure: (1) beam-like particles, (2) elastic and inelastically scattered beam-like particles, (3) particles that reacted in the NaI(Tl) scintillator, (4) proton-picked-up particles, (5) proton-removed particles, (6) beam contaminants, and (7) “out-of-acceptance” particles, which were not detected by the NaI(Tl) detector. The number of

particles with the same Z as the selected incident beam was determined by summing the events in the regions 1, 2 and 3. To estimate the number of light particles in region 3, a Gaussian peak plus an exponential background function was used to fit the experimental data (see Fig. 2(b)). The systematic uncertainties attributed to the background that contribute to the final σ_{CC} 's are below 1 mb for all carbon isotopes.

The main source of systematic uncertainties lies in the estimation of the out-of-acceptance carbon isotopes in the region 7. The particles in the region 7 comprised about 2% of the total events. Simply adopting this value as the systematic uncertainty results in as large as 20% uncertainty in the measured σ_{CC} . Hence, to reduce this uncertainty, we introduced an acceptance-correction factor, denoted by P . The final σ_{CC} was deduced as follows:

$$\sigma_{CC} = \frac{1}{t} \ln \left[\frac{\gamma_{\text{out}}(1 - P_{\text{in}})}{\gamma_{\text{in}}(1 - P_{\text{out}})} \right] \quad (1)$$

where the subscripts ‘‘in’’ and ‘‘out’’ indicate measurements with and without reaction target, respectively. P_i ($i = \text{in}$ or out) was determined by assuming the scattering at large angle as being mainly due to the Rutherford scattering. To determine the experimental P_i , we first calculated the difference in the solid angles ($\Delta\Omega$) covered by a particular MUSIC electrode and the next layer (a MUSIC electrode or the NaI(Tl) scintillator) using the geometrical information of the experimental setup. By taking the event having an appropriate signal in one layer of the MUSIC but not in the next layer as the event

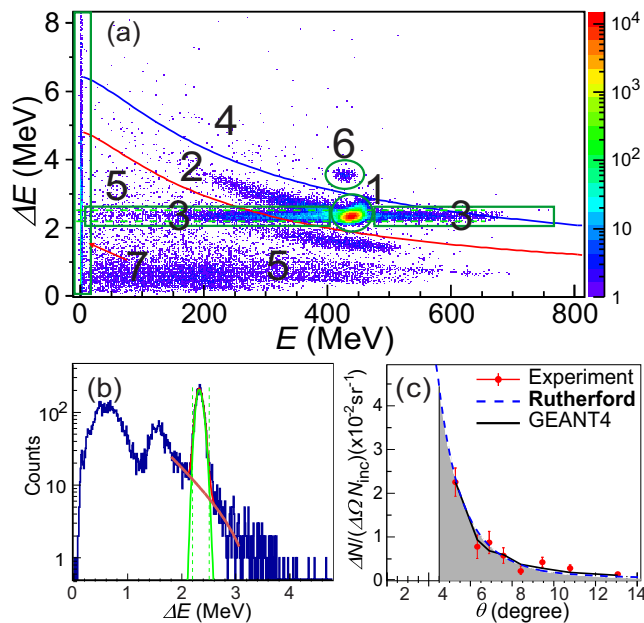


FIG. 2. (Color online). (a) Identification of the scattered particles. (b) Estimation of background contribution from region 5. (c) Acceptance-correction factor calculation. For details see text.

TABLE I. The experimental values of σ_{CC} and proton, neutron rms radii of carbon isotopes.

	E(MeV/u)	σ_{CC} (mb)	r_p^{exp} (fm)	r_p^{ref} (fm)
^{12}C	38.0	1056(20)		
^{12}C	48.4	941(16)	2.35(6) ^a	2.327(7) ^b
^{13}C	47.7	968(39)	2.35(9)	2.321(8) ^b
^{14}C	46.3	960(18)	2.32(4)	2.370(11) ^b
^{15}C	44.1	987(34)	2.41(8)	2.33(11) ^c
^{16}C	44.9	987(20)	2.40(5)	2.25(11) ^c

^a The average value of two energies is shown.

^b From Ref. [45].

^c From Ref. [19].

being scattered into the solid angle $\Delta\Omega$, the number of lost events ΔN was determined for each scattering angle. The $\Delta N/(\Delta\Omega N_{\text{inc}})$ ratios thus obtained are proportional to the differential cross sections of the elastic Coulomb scattering, and were fitted with a calculated Rutherford scattering differential cross section distribution. As shown in the Fig. 2(c), the experimental data are well reproduced by the Rutherford distribution. To further confirm the assumption, we performed Monte Carlo simulations using the Geant4 code [30]. The results from the simulations are also in excellent agreement with the experimental data as well as the Rutherford distribution. The P_i value is simply the integral of the distribution over the solid angles not covered by the NaI(Tl) detectors, as shown by the shaded area in Fig. 2(c). Depending on isotope, the P_{in} (P_{out}) value thus determined varies from 0.003 (0.0005) to 0.004 (0.0012), with an uncertainty between 2 – 10% (5 – 15%). This uncertainties contribute to 6 – 10 mb of σ_{CC} for different isotopes.

The determined σ_{CC} values are summarized in Table I. The uncertainties (in brackets) include the above-mentioned systematic uncertainties, the statistical uncertainties as well as the uncertainty in the target thickness (0.06%). The results for ^{12}C at 38.0-MeV incident energy, measured during the same experiment to examine possible systematic uncertainty due to the incident-beam energy, are also shown.

FORMULATION OF THE GLAUBER MODEL

To extract the proton rms radii, we performed finite-range Glauber-model calculations within the OLA using the parameter set from nucleon–nucleon (N – N) cross sections. Following the procedures in Ref. [17] and ignoring the effect of neutrons in a projectile, we calculate σ_{CC} as follows:

$$\sigma_{CC} = 2\pi \int d\vec{b} \left[1 - |e^{i\chi(b)}|^2 \right] \quad (2)$$

where \vec{b} is the impact parameter, and the exponential term is the transmission function given by the following

relation:

$$e^{i\chi(b)} = \exp \left[\int_{\mathbf{P}} \int_{\mathbf{T}} \sum_N \left[\rho_{\mathbf{P}_p}^z(\vec{s}) \rho_{\mathbf{T}_N}^z(\vec{t}) \Gamma_{\mathbf{p}N}(\vec{b} + \vec{s} - \vec{t}) \right] d\vec{s} d\vec{t} \right].$$

The superscript z in the above formula indicates the direction of integration, which corresponds to the direction of the incident particle, for the nucleon density. $\rho_{\mathbf{P}_p}^z$ is the proton density of the projectile and $\rho_{\mathbf{T}_N}^z$ with subscript $N = \text{p,n}$ is the proton or neutron density of the target. $\vec{s}(\vec{t})$ represents the two-dimensional coordinate of a particular projectile (target) nucleon relative to the center of mass of the projectile (target) nucleus, which lies on the plane perpendicular to the incident momentum of the projectile. Γ is the N - N amplitude [31], which in the case of the scatterings of protons off a nuclear target simplifies as the profile function [23]:

$$\Gamma_{\mathbf{p}N}(\vec{b}) = \frac{1 - i\alpha_{\mathbf{p}N}}{4\pi\beta_{\mathbf{p}N}} \sigma_{\mathbf{p}N}^{\text{tot}} \exp \left[-\frac{b^2}{2\beta_{\mathbf{p}N}} \right] \quad (3)$$

where $\alpha_{\mathbf{p}N}$ is the ratio of the real to the imaginary part of the forward $\text{p}-N$ scattering amplitude, $\beta_{\mathbf{p}N}$ the slope parameter of the $\text{p}-N$ elastic differential cross section, and $\sigma_{\mathbf{p}N}^{\text{tot}}(E)$ is the total $\text{p}-N$ cross section at incident energy E . The energy-dependent $\alpha_{\mathbf{p}N}$ and $\beta_{\mathbf{p}N}$ parameters are interrelated, via the total elastic cross section ($\sigma_{\mathbf{p}N}^{\text{el}}(E)$) and $\sigma_{\mathbf{p}N}^{\text{tot}}(E)$, as follows [32]:

$$\sigma_{\mathbf{p}N}^{\text{el}}(E) = \frac{1 + \alpha_{\mathbf{p}N}^2}{16\pi\beta_{\mathbf{p}N}} [\sigma_{\mathbf{p}N}^{\text{tot}}(E)]^2. \quad (4)$$

In the OLA calculation, only the real part of the profile function that contains only the $\beta_{\mathbf{p}N}$ parameter contributes to the cross section. Hence, it is sufficient to determine β_{pp} and β_{pn} for the Glauber model calculations. Substituting the α_{pp} values and the cross sections from the Particle Data Group tabulation [33] into Eq. 4, we deduced β_{pp} over a wide range of incident energy. For β_{pn} , only a few data points for α_{pn} at incident energies above 174A MeV are available from Ref. [33]. Although parameter sets from the studies on proton-nucleus scatterings at proton energies ranging from 100 to 2200 MeV [31], and on heavy-ion scatterings at projectile energies 30A – 350A MeV [34] are available, both parameter sets failed to reproduce the energy dependence of the reaction/interaction cross section of ^{12}C [22, 35]. Introducing separate parametrization schemes for energies below and above 300A MeV, and adopting partially or modifying the parameters in Ref. [31], several authors have reported improved global systematics [22, 35–37].

In this work, we took a different approach and determined the energy-dependent $\beta_{\text{pn}}(E)$, taking advantage of the accumulating experimental σ_{R} 's [22] of ^{12}C on a ^{12}C target at incident energies from 10A MeV

up to about 2100A MeV. To this end, we first fixed the proton- and neutron-density distributions which are needed for the OLA Glauber calculations. We adopted the sum-of-Gaussian distribution from the electron scattering data [38] as the proton density distribution in the ^{12}C target. For the neutrons, assuming a harmonic-oscillator (HO) type density distribution, we determined the HO width parameter together with β_{pn} so as to reproduce the experimental σ_{R} [39] and σ_{CC} [40] of ^{12}C on a carbon target at around 950A MeV. We chose the data at this energy since the Glauber model is well established for high energies. Using these proton- and neutron-density distributions, we determined the $\beta_{\text{pn}}(E)$ so as to reproduce the experimental σ_{R} at various incident energies. The experimental σ_{R} data (black-open circles) and the “fitted” Glauber model calculation results (black solid line) are shown in Fig. 3(a). The best-fitted $\beta_{\text{pn}}(E)$ is shown in the inset.

RESULTS OF THE GLAUBER-MODEL ANALYSIS AND DISCUSSION

We applied the Glauber model to calculate the σ_{CC} 's at other energies. As shown in Fig. 3(a), the results show good agreement with the experimental σ_{CC} 's in the whole energy range including our measurements (red-filled squares). Using the same $\beta_{\text{pn}}(E)$ and density distribution of ^{12}C , we also calculated $\sigma_{\text{R}}(E)$ for ^{12}C on beryllium and aluminum targets. Again, we adopted the shape of distribution suggested from the electron-scattering data [38] for the proton density distributions of ^9Be and ^{27}Al . For the neutrons, we assumed a harmonic-oscillator (HO) plus Woods-Saxon (WS) shape for the Be and a WS shape density distributions for the Al target nuclei, namely:

$$\rho_{\text{Be}} = \rho_{\text{HO}}(N=4, R_{\text{Be}}, r) + \rho_{\text{WS}}(N=1, R_{\text{Be}}, a_{\text{Be}}, r), \quad (5)$$

$$\rho_{\text{Al}} = \rho_{\text{WS}}(N=14, R_{\text{Al}}, a_{\text{Al}}, r), \quad (6)$$

where

$$\rho_{\text{HO}}(N, R, r) = \rho_0^{\text{HO}} \exp \left[-\left(\frac{r}{R}\right)^2 \right] \left[1 + \frac{N-2}{3} \left(\frac{r}{R}\right)^2 \right],$$

$$\rho_{\text{WS}}(N, R, a, r) = \frac{\rho_0^{\text{WS}}}{1 + \exp[(r-R)/a]}$$

ρ_0^{HO} and ρ_0^{WS} are normalization factors that conserve number of neutron(s). Here, we introduced the Woods-Saxon distribution with a tail density to account for the loosely-bound valence neutron in ^9Be , and determined the diffuseness as well as the HO width parameter for the ^9Be target so as to reproduce the experimental data at 33.6A [41] and 921A MeV [39]. For the ^{27}Al target, σ_{R} 's

at 40.2A and 372.4A MeV [41] were used to determine the WS parameters. As shown in Fig. 3(b), our calculations are in excellent agreement with the experimental data of ^{12}C on beryllium and aluminum targets. We note that calculations using the formulation [42] that includes higher order corrections to the OLA yield only slightly different results which are consistent with the OLA calculations within the experimental uncertainties (see the dashed lines in Fig. 3(a)).

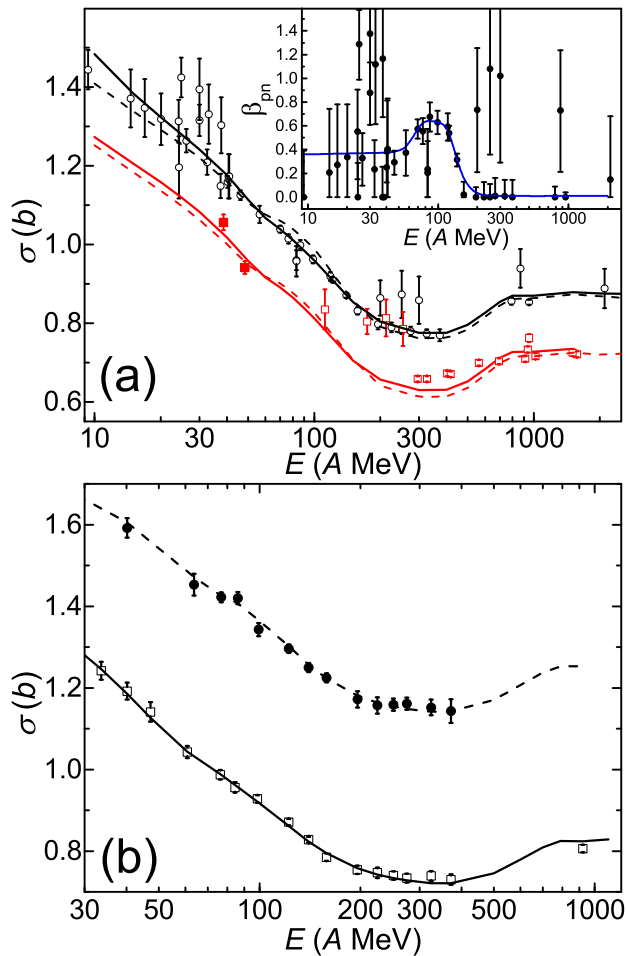


FIG. 3. (Color online). (a) Experimental σ_R 's (black-open circles) [39, 41] and σ_{CC} 's (red symbols) of ^{12}C on carbon target. The red-filled and red-open squares are our data at 45A MeV and data from Ref. [40, 43] respectively. The black solid line is the energy-dependent $\sigma_R(E)$ calculated with the best-fitted $\beta_{pn}(E)$ (inset) and HO-type neutron density distribution. The red solid line is the calculated $\sigma_{CC}(E)$. The dashed (black and red) lines are results of Glauber calculations (for $\sigma_R(E)$ and $\sigma_{CC}(E)$) with the OLA plus higher-order correction [42]. (b) Experimental σ_R 's for ^{12}C on a beryllium (open squares) and aluminum (filled circles) targets. The solid and dashed lines are the $\sigma_R(E)$'s calculated with the present Glauber model. A neutron-density distribution with a tail structure is necessary for beryllium target. See text for the details on the input density distributions for the target nucleons.

Figure 4 shows the experimental σ_{CC} 's (red symbols) and σ_R 's (black symbols) of (a) ^{14}C and (b) ^{16}C on a ^{12}C target. The red-filled squares are our data at around 45A MeV. The red-open squares are the data taken from Refs. [19, 43]. The black-open circles are the σ_R data taken from Refs. [39, 41]. To calculate the $\sigma_R(E)$ and $\sigma_{CC}(E)$, and to extract the proton and neutron rms radii, we assumed HO-type proton-density distributions for the protons and neutrons in ^{14}C . We used the σ_R data at 950A MeV [39] and our σ_{CC} to determine the HO width parameters for the proton- and neutron-density distributions. We have avoided using the other σ_{CC} data shown in Fig. 4(a) because we found systematic deviations from our data for all $^{12-16}\text{C}$ isotopes. We note that the σ_{CC} at around 930A MeV from Ref. [43] deviates as much as 7% from the datum at around 950A MeV from Ref. [40], which we have used together with the σ_R at 950A MeV to determine the global parameters. In addition, we have also confirmed that our calculations can reproduce the recent σ_{CC} data for all carbon isotopes at around 900A MeV [44]. The $\sigma_{CC}(E)$ and $\sigma_R(E)$ thus calculated are shown by the red-dashed and the black lines in Fig. 4(a).

For the ^{16}C isotope, a ^{14}C -core-plus-two-neutron type nucleon density distribution has been suggested. Assuming such density distribution, T. Zheng *et al.* deduced a nucleon-density distribution with a relatively long tail [25]. Here, as a first trial, we assumed the HO-type density distributions similar to ^{14}C . The proton- and neutron-density distributions required to reproduce the experimental σ_R at around 950A MeV and our σ_{CC} are shown by the red-dashed and black-solid lines respectively. Obviously, the calculated $\sigma_R(E)$ underestimates the two experimental σ_R 's at energies below 100A MeV. Such deviation is well known and has been observed in the reactions of ^{11}Be on ^{12}C and ^{27}Al at 33A-MeV incident energy [24]. To reproduce the experimental σ_R at low energy, we considered the HO core plus WS-type-two-neutron tail (core+2n) density distribution. The parameters for the core+2n neutron-density distribution were determined so as to reproduce the experimental σ_R 's at 39A [46] and 950A [39] MeV. The core+2n density distribution thus deduced is shown by the black-dotted line in the inset of Fig. 4(b). The calculation also reproduces the experimental data at 83A MeV [25] very well. We note that similar neutron-density distribution, i.e. HO core plus WS-type-one-neutron tail (core+n), is also required to reproduce the sole σ_R datum for ^{15}C at around 20A MeV [46]. However, the experimental uncertainty is too large to allow any definite conclusion. Hence, the present results confirm the importance of the σ_R (and perhaps the σ_{CC}) measurements at incident energies below 100A MeV.

The proton rms radii for $^{12-16}\text{C}$ thus extracted from our measured σ_{CC} 's are also shown in Table I. For comparison, the experimental proton rms radii for $^{12-14}\text{C}$

from the electron-scattering data [45] and $^{15-16}\text{C}$ from Ref. [19] are also shown. The uncertainties of proton rms radii shown in Table I are from the uncertainties of σ_{CC} 's, and do not include those of β_{pn} , which are mainly from σ_{R} 's. In this energy region, the uncertainty of σ_{R} is almost equivalent to that of our σ_{CC} . Including these uncertainties results in an additional uncertainty factor of about $\sqrt{2}$ in proton rms radii, which will not affect our conclusion. It is important to note that our results for $^{12-14}\text{C}$ are in good agreement with, within one standard deviation from, the electron-scattering data. These

agreements provide further justification for the adoption of our experimental σ_{CC} 's in determining the density distributions. The general consistencies between the experimental (σ_{R} and σ_{CC}) cross sections and our Glauber-model calculations with global parameters demonstrate the validity and versatility of the model for various isotopes over a wide range of incident energies.

SUMMARY

In summary, we have measured the σ_{CC} 's of $^{12-16}\text{C}$ on a carbon target using the transmission method at around 45A MeV incident-beam energies at the RCNP EN course, Osaka University. To analyze the low-energy data, we have developed a finite-range Glauber model with a global parameter set within the optical-limit approximation, which is applicable to incident energies below 100A MeV. Our calculations show excellent agreement with the experimental σ_{R} 's for reactions of ^{12}C on a ^9Be and ^{27}Al targets. Performing the Glauber-model analysis on the experimental σ_{R} and σ_{CC} , we show the sensitivity of the low-energy σ_{R} to the tail-density distribution of “neutron-halo” or “neutron-skin” nuclei. The results confirm the importance of the σ_{R} (and perhaps σ_{CC}) measurements at incident energies below 100A MeV. We also extracted the proton rms radii for $^{12-16}\text{C}$ using our measured σ_{CC} 's and the existing σ_{R} data. The results for $^{12-14}\text{C}$ are in good agreement with the values from the electron scatterings. These consistencies, together with the capability of our calculations to reproduce most of the experimental σ_{R} and σ_{CC} data for several isotopes and over a wide range of incident energies, demonstrate the usefulness of the σ_{CC} measurement and our Glauber model.

ACKNOWLEDGEMENTS

We thank the RCNP Ring Cyclotron staff for delivering ^{22}Ne beam stably throughout the experiment, and Prof. K. Kimura for his precious advice during the preparation of the MUSIC detector. H.J.O. and I.T. would like to acknowledge the support of Prof. A. Tohsaki (Suzuki) and his spouse. D.T.T. and T.T.N. appreciate the support of RCNP Visiting Young Scientist Support Program. The support of the Vietnam government under the Program of Development in Physics by 2020, the PR China government and Beihang University under the Thousand Talent Program, and the supports from the Nishimura and Hirose International Scholarship Foundations are gratefully acknowledged. This work was supported in part by JSPS-VAST Bilateral Joint Research Project and Grand-in-Aid for Scientific Research Nos. 20244030, 20740163, 23224008 from Monbukagakusho, Japan.

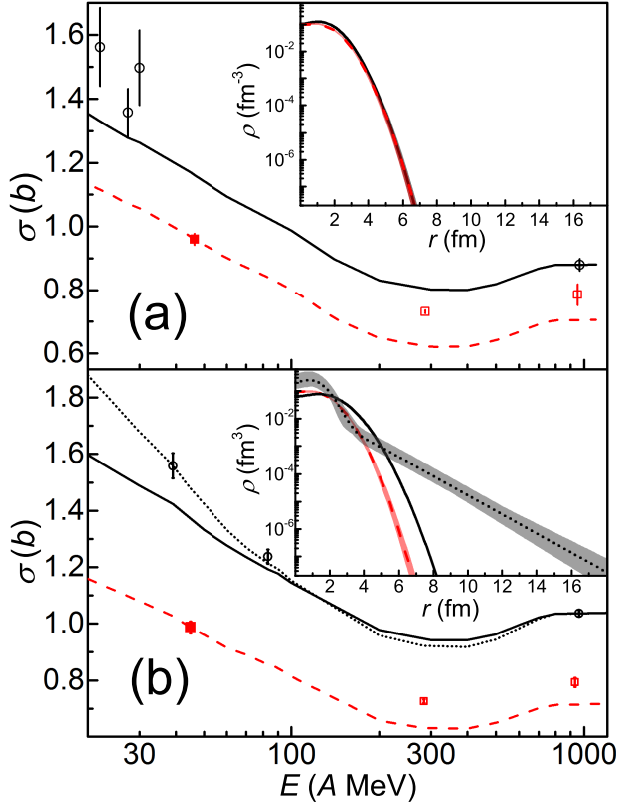


FIG. 4. (Color online). Experimental σ_{CC} 's (red symbols) and σ_{R} 's (black symbols) of (a) ^{14}C and (b) ^{16}C on a ^{12}C target. The red-filled squares are our data at around 45A MeV. The red-open squares are the data taken from Refs. [19, 43]. The black-open circles are the σ_{R} data taken from Refs. [39, 41]. The red-dashed and the black lines correspond to the $\sigma_{\text{CC}}(E)$ and $\sigma_{\text{R}}(E)$ calculated using the present Glauber model. We assumed HO-type density distributions for the protons and neutrons in ^{14}C , as well as for the protons in ^{16}C . For ^{16}C , the neutron-density distribution with a HO core plus WS-type-two-neutron tail (core+2n) is necessary to reproduce the σ_{R} at energy below 100A MeV. The proton- and neutron-density distributions thus determined are shown in the insets: the red-dashed (black-solid) lines represent the HO-type proton- (neutron-) density distributions, and the black-dotted line represent the core+2n neutron-density distribution. The hatched areas represent the uncertainties in the density distributions due to the uncertainties in the measured cross sections.

-
- * tdtrong@rcnp.osaka-u.ac.jp
† onghjin@rcnp.osaka-u.ac.jp
- [1] B.A. Brown, Phys. Rev. Lett. **85**, 5296 (2000).
[2] J. M. Lattimer, Annu. Rev. Nucl. Part. Sci. **62**, 485 (2012).
[3] G. Gamow and C. L. Critchfield, *Atomic nucleus and nuclear energy source*, Clarendon Press, Oxford (1949).
[4] L. R. B. Elton, *Nuclear sizes*, Oxford Uni. Press, (1961).
[5] M. Wakasugi *et al.*, Nucl. Instr. Methods Phys. Res. **B317**, 668 (2013).
[6] P. Campbell *et al.*, Prog. Part. Nucl. Phys. **86**, 127 (2016).
[7] L. -B. Wang *et al.*, Phys. Rev. Lett. **93**, 142501 (2004).
[8] R. Sanchez *et al.*, Phys. Rev. Lett. **96**, 033002 (2006).
[9] P. Mueller *et al.*, Phys. Rev. Lett. **99**, 252501 (2007).
[10] W. Nörtershäuser *et al.*, Phys. Rev. Lett. **102**, 062503 (2009).
[11] A. Takamine *et al.*, Phys. Rev. Lett. **112**, 162502 (2014).
[12] A. Krieger *et al.*, Phys. Rev. Lett. **108**, 142501 (2012).
[13] I. Tanihata *et al.*, Phys. Rev. Lett. **55**, 2676 (1985).
[14] R. J. Glauber, in *Lectures in Theoretical Physics*, Interscience, New York, Vol 1, p. 315 (1959).
[15] A. Ozawa *et al.*, Nucl. Phys. A **693**, 32 (2001).
[16] I. Tanihata *et al.*, Prog. Part. Nucl. Phys. **68**, 215 (2013).
[17] S. Terashima *et al.*, Prog. Theor. Exp. Phys. **101D02**, (2014).
[18] A. Estrade *et al.*, Phys. Rev. Lett. **113**, 132501 (2014).
[19] T. Yamaguchi *et al.*, Phys. Rev. Lett. **107**, 032502 (2011).
[20] M. Takechi *et al.*, Eur. Phys. J. A **25**, 217 (2005).
[21] N. J. DiGiacomo, R. M. DeVries, and J. C. Peng, Phys. Rev. Lett. **45**, 527 (1980); Phys. Lett. **101B**, 383 (1981).
[22] M. Takechi *et al.*, Phys. Rev. C **79**, 061601 (2009).
[23] B. Abu-Ibrahim and Y. Suzuki, Phys. Rev. C **62**, 034608 (2000).
[24] M. Fukuda *et al.*, Phys. Lett. B **268**, 339 (1991).
[25] T. Zheng *et al.*, Nucl. Phys. A **709**, 103 (2002).
[26] T. Shimoda *et al.*, Nucl. Instr. Methods Phys. Res. **B70**, 320 (1992).
[27] H.J. Ong *et al.*, RCNP Ann. Rep., 17 (2011).
[28] H. Kumagai *et al.*, Nucl. Instr. Methods Phys. Res. **A470**, 562 (2001).
[29] K. Kimura *et al.*, Nucl. Instr. Methods Phys. Res. **A538**, 608 (2005).
[30] S. Agostinelli *et al.*, Nucl. Instr. Methods Phys. Res. **A506**, 250 (2003).
[31] L. Ray, Phys. Rev. C **20**, 1857 (1979).
[32] Y. Ogawa *et al.*, Nucl. Phys. A **543**, 722 (1992).
[33] K.A. Olive *et al.* (Particle Data Group), Chin. Phys. C, **38**, 090001 (2014) and 2015 update.
[34] S. M. Lenzi, A. Vitturi and F. Zardi, Phys. Rev. C **40**, 2114 (1989).
[35] W. Horiuchi *et al.*, Phys. Rev. C **75**, 044607 (2007).
[36] B. Abu-Ibrahim *et al.*, Nucl. Phys. A **657**, 391 (1999).
[37] B. Abu-Ibrahim *et al.*, Phys. Rev. C **77**, 034607 (2008).
[38] H. De Vries, *et al.*, At. Data Nucl. Data Tables **36**, 495 (1987).
[39] A. Ozawa *et al.*, Nucl. Phys. A **691**, 599 (2001).
[40] W.R. Webber *et al.*, Phys. Rev. C **41**, 520 (1990).
[41] M. Takechi, Ph.D. thesis, Osaka University, 2006.
[42] B. Abu-Ibrahim *et al.*, Phys. Rev. C **61**, 051601 (2000).
[43] L.V. Chulkov *et al.*, Nucl. Phys. A **674**, 330 (2000).
[44] R. Kanungo *et al.*, submitted for publication.
[45] I. Angeli, K. P. Marinova, At. Data Nucl. Data Tables **99**, 69 (2013).
[46] D.Q. Fang *et al.*, Phys. Rev. C **61**, 064311 (2000).